Reheating of the Universe and Population III

Jeremiah P. Ostriker[1] and Nickolay Y. Gnedin[1,2]

ABSTRACT

We note that current observational evidence strongly favors a conventional recombination of ionized matter subsequent to redshift $z = 1200$, followed by reionization prior to redshift $z = 5$ and compute how this would have occurred in a standard scenario for the growth of structure. Extending prior semi-analytic work, we show by direct, high-resolution numerical simulations (of a *COBE* normalized CDM+Λ model) that reheating, will occur in the interval $15 > z > 7$, followed by reionization and accompanied by a significant increase in the Jeans mass. However, the evolution of the Jeans mass does not significantly affect star formation in dense, self-shielded clumps of gas, which are detached from the thermal evolution of the rest of the universe. On average, the growth of the Jeans mass tracks the growth of the nonlinear mass scale, a result we suspect is due to nonlinear feedback effects. Cooling on molecular hydrogen leads to a burst of star formation prior to reheating which produces Population III stars with Ω_* reaching $10^{-5.5}$ and $\bar{Z}/Z_\odot$ reaching $10^{-3.7}$ by $z = 14$. Star formation subsequently slows down as molecular hydrogen is depleted by photo-destruction and the rise of the temperature. At later times, $z < 10$, when the characteristic virial temperature of gas clumps reach 10^4 degrees, star formation increases again as hydrogen line cooling become efficient. Objects containing Pop III stars accrete mass with time and, as soon as they reach 10^4 K virial temperature, they engage in renewed star formation and turn into normal Pop II objects having an old Pop III metal poor component.

Subject headings: cosmology: theory - cosmology: large-scale structure of universe - galaxies: formation - galaxies: intergalactic medium

1. Introduction

In the standard, hot big bang model of cosmology, radiation and matter decouple from one another at approximately redshift $z \approx 1200$ with recombination proceeding until the ionized fraction freezes out at $n_e/n_{\rm H\,I} \approx 4 \times 10^{-4}$ at about redshift $z \approx 800$ (cf. Peebles 1993). But we know from the classic Gunn-Peterson test (Gunn & Peterson 1965), that the universe is again ionized at low redshifts with

[1]Princeton University Observatory, Peyton Hall, Princeton, NJ 08544;
e-mail: *jpo@astro.princeton.edu*

[2]Department of Physics, Massachusetts Institute of Technology, Cambridge, MA 02139; e-mail: *gnedin@arcturus.mit.edu*

the neutral fraction still below 6×10^{-6} at redshift $z \approx 4$ (Jenkins & Ostriker 1991; Giallongo et al. 1994). In this standard picture reionization must occur, due to unknown sources in the intervening time interval. The purpose of the present paper is to indicate how and when this happens according to present theories for the development of structure. This work differs from prior papers on this subject primarily in two respects: (1) we treat (imperfectly but) in greater detail than has been done previously many of the relevant physical processes such as molecular hydrogen formation, spectrum of the ambient radiation field, absorption etc, and (2) we allow explicitly for the density inhomogeneities that develop through the action of gravity and pressure using the SLH code of Gnedin (1995) as modified by Gnedin & Bertschinger (1996).

Many authors have studied this process, from the pioneering work of Couchman & Rees (1986), Shapiro (1986a, 1986b) to the recent careful investigations by Tegmark and Silk (1994, 1995), Kawasaki & Fukigita (1994), Giroux & Shapiro (1996), Tegmark et al. (1996) and others. While varying amounts of physically detailed modelling were included in all of those papers, there was a critical factor that could not be followed in any of the semi-analytic treatments: the clumping of the gas. But all relevant processes are dependent on the clumping factor $\eta \equiv \langle\rho^2\rangle/\langle\rho\rangle^2$. Included among these processes are *recombination, cooling, gravitational collapse, molecular hydrogen formation* and numerous others. Thus a fully nonlinear three dimensional threatment appears to be warranted. That is what we have undertaken, using one of the currently plausible models for the growth of structure - the CDM+Λ model (cf. Ostriker & Steinhardt 1995 for references) as a point of departure. The Jeans mass after decoupling for gas at the CBR temperature is constant and has the value of $1.7 \times 10^6 h^{-1}\,\mathrm{M}_\odot$. After redshift approximately 100, the gas temperature is no longer coupled to the CBR temperature, and the Jeans mass decreases as $(1+z)^{3/2}$, approaching the value of $5.4 \times 10^4 h^{-1}\,\mathrm{M}_\odot$ at $z = 10$. So, it is necessary to perform simulations with at least this mass resolution. The work reported on here adopts the the model and numerical parameters given in Table 1 (close to the "concordance" model of Ostriker & Steinhardt 1995), but the dependence of our quoted results on the assumed scenario is, we expect, small. With a box size of $2h^{-1}\,\mathrm{Mpc}$ and a Lagrangian resolution for the SLH code (Gnedin 1995; Gnedin & Bertschinger 1996) of 128^3 which corresponds to a gas mass of $\Delta M_g = 3.2 \times 10^4 h^{-1}\,\mathrm{M}_\odot$ and a dark matter particle mass of $\Delta M_d = 3.7 \times 10^5 h^{-1}\,\mathrm{M}_\odot$, we have marginally resolved the smallest self-gravitating structures. Spatial resolution in our fiducial run is approximately $1h^{-1}\,\mathrm{kpc}$.

A detailed description of the physical modelling will be presented in Gnedin & Ostriker (1996). Here we note that we have allowed for the formation and destruction of molecular hydrogen, as well as all other standard physical processes for a gas of primeval composition, following in detail the ionization and recombination of all species in the ambient radiation field. The spatially averaged but frequency dependent radiation field, in turn, allows for sources of radiation (quasars and massive stars), sinks (due to continuum opacities) and cosmological effects. In regions which are cooling and collapsing we have allowed the formation of point-like "stellar" subunits, permitting them to release radiation and (in proportion) metal rich gas, which we have considered in the treatment of cooling. Finally, we have taken into account the fact that dense lumps will be shielded from the background radiation field. This reduces the heating rates for dense clumps and makes it nearly certain that once they have formed and started to collapse, the process will be irreversible.

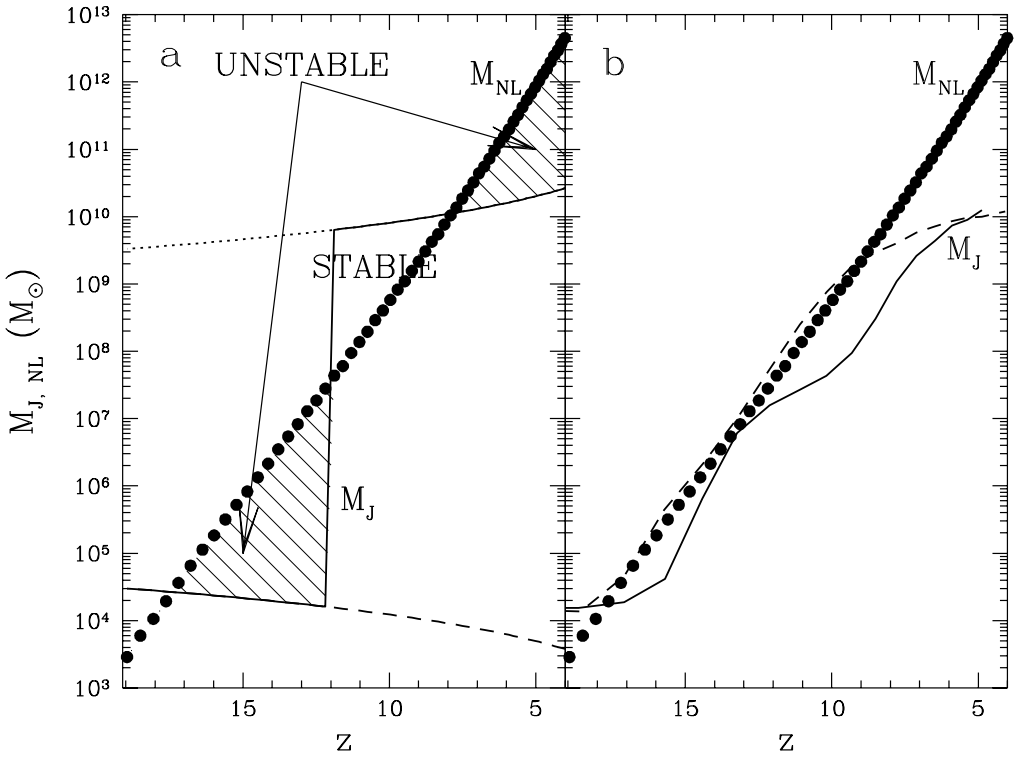

Fig. 1.— *a)* The Jeans mass for the adiabatically expanding intergalactic gas (*dashed line*), gas at 10^4 K (*dotted line*), and transition curve for instantaneous reheating (*solid line*). Dots show the nonlinear mass. *b)* The nonlinear mass (*filled dots*) and the Jeans mass from run A (*solid line*) and run B (*dashed line*).

2. A Qualitative Approach to Reionization

Let us first ignore reheating and estimate the rate at which matter would begin to collapse following the standard theories of gravitational instability such as the Press-Schechter picture (1974). For cold gas in CDM-like theories at first no mass elements are unstable to collapse. Then as gravitational instability grows, higher and higher mass scales will become unstable, as indicated by the line made of heavy dots in Fig.1a.

Now consider the Jeans mass, the mass above which the self-gravitating gas at the cosmic density and temperature would be unstable. The dashed curve in Fig.1a shows gas at the CBR temperature and the dotted curve marks the gas at 10^4 K, with a schematic transition curve indicated by the solid curve for gas that heats rapidly to 10^4 K at $z = 12$, when, we hypothesize, ionization and reheating occur in this schematic treatment. We see that we might expect there to be an epoch of instability to exist before reheating and reionization, when low mass objects collapse out of cold gas (left hatched

Table 1: Model and Numerical Parameters

Run	N	Box size	Total mass res.	Spatial res.	Dyn. range
A	128^3	$2h^{-1}\,\mathrm{Mpc}$	$3.7\times10^5h^{-1}\,\mathrm{M}_\odot$	$1.0h^{-1}\,\mathrm{kpc}$	2000
B	64^3	$2h^{-1}\,\mathrm{Mpc}$	$2.9\times10^6h^{-1}\,\mathrm{M}_\odot$	$3.0h^{-1}\,\mathrm{kpc}$	640
C	64^3	$1h^{-1}\,\mathrm{Mpc}$	$3.7\times10^5h^{-1}\,\mathrm{M}_\odot$	$1.5h^{-1}\,\mathrm{kpc}$	640

region) and another, later epoch, when galactic mass objects condense out of $10^4\,\mathrm{K}$ gas (right hatched region), which are separated in time by a region during which gas is stable against gravitational collapse. A diagram of this type was computed and shown in Cen, Ostriker, & Peebles (1993; Fig.8) to illustrate, quantitatively, the epochs at which star and galaxy formation would occur in the PBI model.

This early population of stars that formed before reheating may be considered a candidate for a relatively smoothly distributed Population III. One expect that these stars will mostly reside in low mass systems ($M_{\rm tot}\lesssim 10^{7.5}\,\mathrm{M}_\odot$, $M_*\lesssim 10^6\,\mathrm{M}_\odot$) which will contaminate the universe with a first generation of metals (to $Z/Z_\odot\sim10^{-4}$ by redshift of around 10). After the Jeans mass increases significantly, normal galaxy formation would occur with masses $M_{g,\rm tot}>10^{10}\,\mathrm{M}_\odot$, $M_{g,*}>10^8\,\mathrm{M}_\odot$ from gas already pre-enriched with metals (Population II). However, as we shall see, while there are elements of truth to the scenario indicated by Figure 1a, the real situation is far more complex.

3. Results

We have performed three different simulations (cf Table 1) with different box sizes and resolution to assess the importance of different scales and estimate the uncertainty due to the finite resolution of our simulations. We fix cosmological parameters as follows: $\Omega_0=0.35$, $h=0.7$, and $\Omega_b=0.03$. The largest of our simulations, run A, is our fiducial run against which to compare results of the two smaller runs. However, it happened by accident that the particular realization of initial conditions we used for run A had substantially less power on large scales ($1-2h^{-1}\,\mathrm{Mpc}$) than the true power spectrum, and we have to take this fact into account when interpreting our results.

3.1. Evolution of Jeans and Nonlinear Mass and Population III

In the real universe, unlike the oversimplified picture illustrated in Fig.1a, there are inhomogeneities on a range of scales, so each small piece of the universe would evolve according to its local values of the Jeans and nonlinear mass. But different pieces are not correlated, so we must appropriately average Fig.1a over the whole distribution of densities and temperatures in the universe to compute the evolution of the average Jeans and nonlinear mass, with the result being that the two separate epochs of star formation would merge and the Jeans mass, instead of jumping over the nonlinear mass in one sudden reheating, would instead trace the nonlinear mass closely in a self-regulating fashion.

The Fig.1b, our computed result, illustrates this conclusion. In this figure we again mark with dots the nonlinear mass, and Jeans mass from runs A (the solid curve) and B (the dashed curve) are plotted on top of the nonlinear mass. We notice that they closely follow each other from $z = 17$ to $z = 10$. There are not two distinct epochs of star formation separated by the period of reheating. Averaged globally, the Jeans mass, due to feedback, traces the evolution of the nonlinear mass scale. Too high a rate of star formation produces too large a fraction of the universe at 10^4 K with, consequently, too high an average Jeans mass suppressing star formation – and conversely. But, as we shall see, there is a more complicated scenario, dependent on molecular cooling, which does produce an early Pop III.

3.2. Population II and Population III

We now proceed to study individual objects formed in simulations. For all bound objects identified with the DENMAX algorithm (Bertschinger & Gelb 1991) and containing more than 100 particles we compute their properties like the total mass $M_{\rm tot}$, the total baryonic mass $M_{\rm b}$, the mass in stars M_*, the mass of metal-enriched gas M_Z, the average redshift of star formation $z_{\rm form}$ computed according to the following formula $\log(1 + z_{\rm form}) \equiv \sum_* m_* \log(1 + z_*)/\sum_* m_*$, where the sum is over all star particles in the object, and z_* is the redshift of a star particle formation, and possibly other properties.

We now plot in Fig.2 distributions of $M_{\rm tot}$, $M_{\rm b}$, M_*, and M_Z as a function of $z_{\rm form}$ for all bound object with more than 100 particles identified at $z = 4.4$ in run A. The distribution is obviously bimodal, and to stress that, we plot all objects whose stars formed at $z > 10$ with open circles and all objects whose stars formed after $z = 10$ with solid squares. According to the KS test, the probability that distributions of total masses for $z > 10$ and $z < 10$ objects are drawn from the same random distribution is infinitesimal. Thus, there indeed exist two populations of objects, which we will call Population II ($z_{\rm form} > 10$) and Population III ($z_{\rm form} < 10$), but not due to the evolution of the Jeans mass. Distributions from runs B and C both show the same property, except that the run B has only a handful of Pop III objects.

In order to understand the appearance of two populations, we first concentrate on their evolution. We identify all bound objects with more than 100 particles at redshift $z = 12.1$. Those are plotted as open circles in Fig.3 and the vertical line with the open circle at the bottom shows the redshift $z = 12.1$. According to our criterion, they are all Pop III objects at that time. We now track the evolution of those objects in ($M_{\rm tot}$,$z_{\rm form}$) plane and plot them with stars at $z = 7.1$ and with solid squares at $z = 4.3$. It is apparent that with time Pop III objects are turning into Pop II.

This conclusion is not surprising if we recall that star formation is occurring in all objects, and younger stars, formed after $z = 10$, would drag the $z_{\rm form}$ label to lower redshifts. However, this does not explain the presence of a gap between Pop II and Pop III. If the star formation rate were continuous over the time, there would be a continuous distribution of objects with respect to $z_{\rm form}$. Therefore, we must conclude that there existed two epochs of star formation, the first initial burst at $z \sim 14$, and the following continuous star formation at $z < 10$. Since the existence of those two epochs cannot be explained by the evolution of the Jeans mass, we must search for another reason for it.

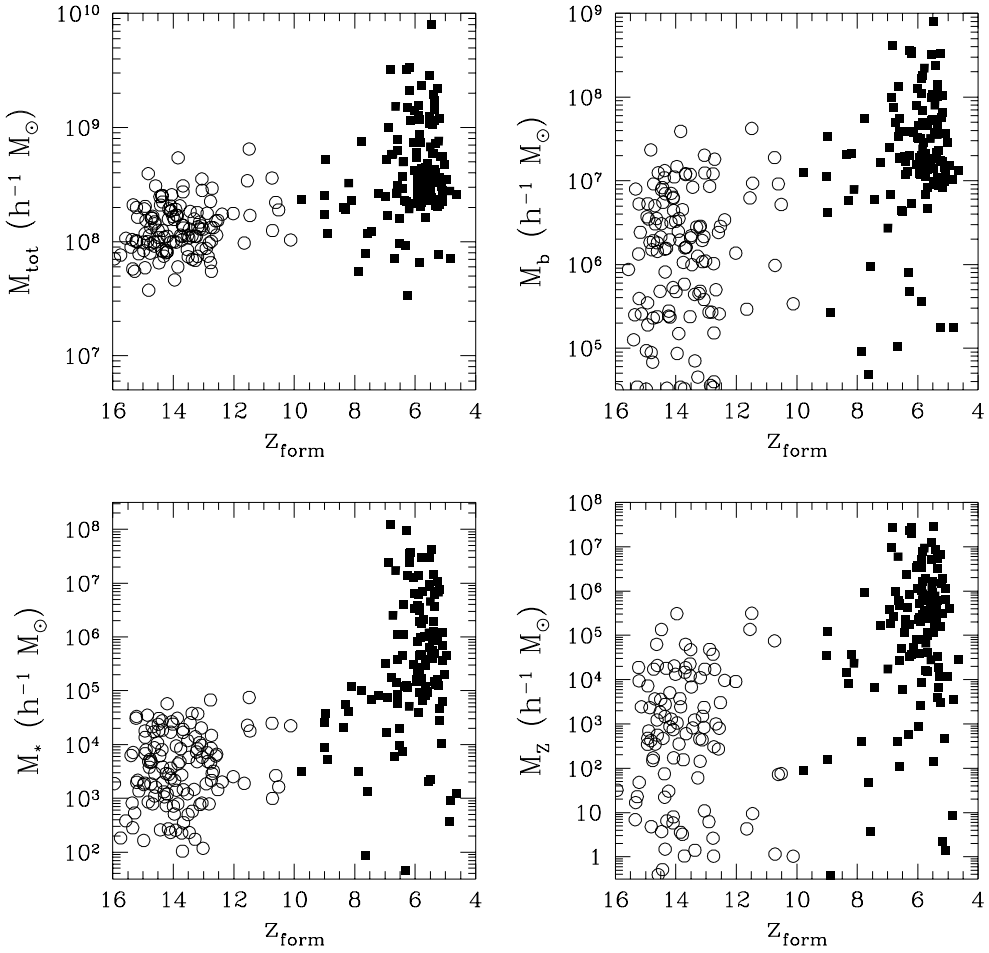

Fig. 2.— Total mass $M_{\rm tot}$ (*upper left panel*), baryonic mass $M_{\rm b}$) (*upper right panel*), stellar mass M_*) (*lower left panel*), and the mass in metals M_Z) (*lower right*) as a function of average redshift of star formation for all bound objects with more than 100 particles at $z = 4.3$. Open circles and filled squares show Pop III and Pop II respectively.

3.3. Physical Mechanism for the Formation of Population III

Radiative cooling of gas is responsible for eventual gas collapse and star formation. In Fig.4 we plot the star formation rates for run A (solid lines) and run B (dashed lines). For each run we show as a heavy line the actual star formation rate, and in the thin line the star formation rate that we would compute assuming that the cooling time is infinitely short. For run B the difference is very small and only exists at $z = 14 - 17$, whereas for run A there exist two distinct epochs of star formation which disappear if the cooling time is set to zero. Also, shown with the thin dotted line is the star formation rate computed from Press-Schechter formalism assuming that all gas in halos with the virial temperature above $1.5 \times 10^4\,{\rm K}$ form stars.

By the time the first epoch of star formation is completed, $z = 14$, the density parameter in stars, Ω_* is reaching $10^{-5.5}$, and the metal contamination is reaching $\bar{Z}/Z_\odot \sim 10^{-3.7}$.

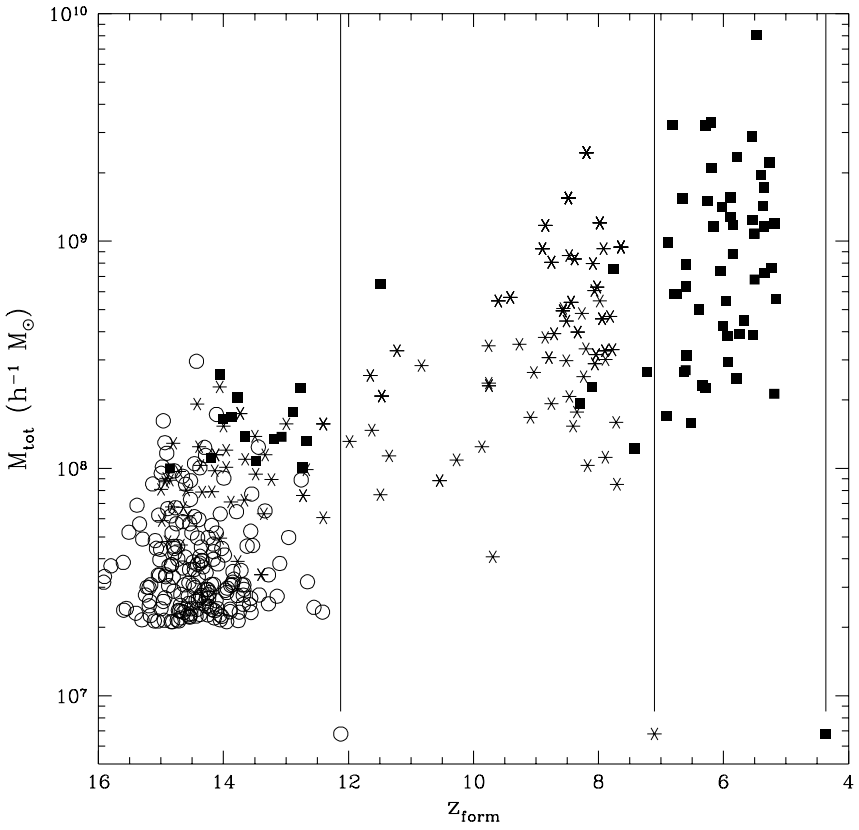

Fig. 3.— Distribution of all bound objects with more than 100 particles identified at $z = 12.1$ in ($M_{\rm tot}$,$z_{\rm form}$) plane for three different redshifts: $z = 12.1$ (*open circles*), $z = 7.1$ (*stars*), and $z = 4.3$ (*filled squares*). Vertical lines with symbols mark correspondent redshifts. Note that two populations continue to exist at both latter epochs but continued star formation depletes the pure Pop III groups.

In order to understand the difference in cooling at high and low redshift we compute the temperature and density for each star particle at the moment it was created. Fig.5 shows joint distributions of all star particles in $[T(z_{\rm form}),z_{\rm form}]$ plane for the fiducial run A. Two epochs of star formation are easily observed in Fig.5. The careful examination of Fig.5 reveals that the early peak corresponds to the temperatures around 10^3 K. Since the only cooling mechanism which exists at these temperatures in the plasma of primeval composition is molecular hydrogen, we therefore conclude that Population III stars formed at $z > 14$ from primeval gas that collapsed losing it energy by exiting rotational and vibrational levels of hydrogen molecules, and Population II stars formed later from gas that collapsed, losing its energy mainly by exiting hydrogen atomic lines. A detailed study of individual objects confirms that early star formation is driven by H_2 cooling.

To illustrate this effect further, we show in Fig.6 with heavy dots the cooling function of the primeval gas containing 10^{-3} of molecular hydrogen my mass at low temperature (at higher temperatures, $T > 4,000$ K, the destruction of molecular hydrogen is taken into account). The thin line shows the value the cooling function should have in order for a virialized object with given temperature to cool in a Hubble time. This figure can only be considered as an illustration since it is based on

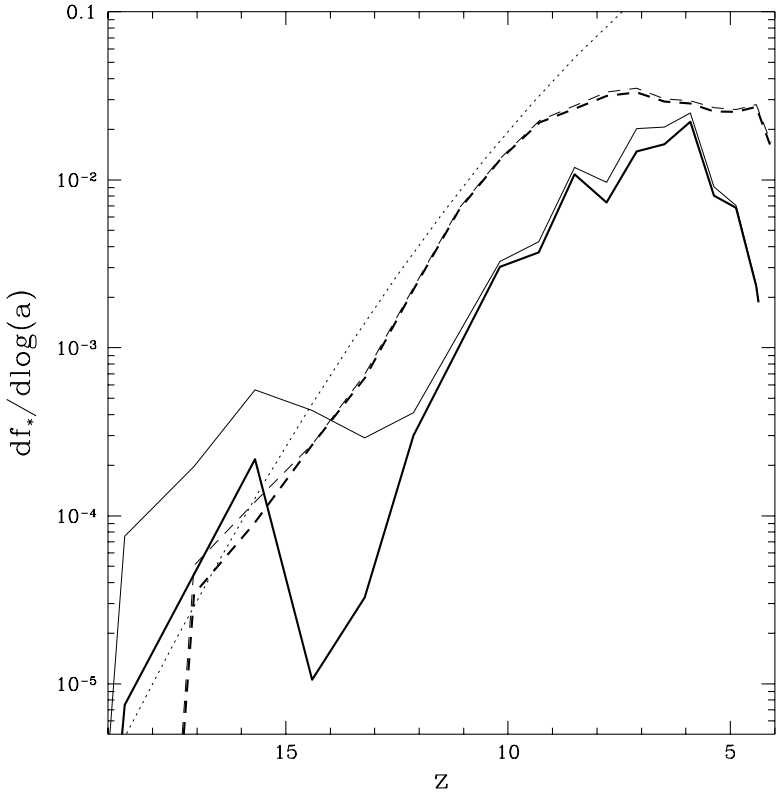

Fig. 4.— The star formation rate for run A (*solid lines*) and run B (*dashed lines*) as a function of redshift. Bold lines show the star formation rate as computed, and thin lines show the star formation rate as would be computed if the cooling time were infinitely short. Thin dotted line shows the rate with which the mass fraction of all halos with the virial temperature above 1.5×10^4 K increases as computed from the Press-Schechter formalism.

the same oversimplified line of arguments as presented in §2. However, it indicates that molecular hydrogen cooling is relatively more efficient at higher redshifts.

4. Conclusions

We have demonstrated by means of detailed cosmological hydrodynamic simulations, which includes an accurate treatment of atomic physics and chemistry of the primeval hydrogen-helium plasma, accounts approximately for the self-shielding of the gas and cooling on metals, and incorporates phenomenological approach to star formation, that the evolution of the Jeans mass during reheating of the universe does not lead to formation of two distinct populations of stars: Pop II and Pop III, but, instead, tracks the nonlinear mass due to feedback effects consequent to star formation. Nevertheless, the two distinct populations of stars form, for a completely different physical reason: the first generation of stars formed when molecular hydrogen cooling was important before $z = 14$, and after molecular hydrogen was depleted by the rise of the virial temperature in most of objects

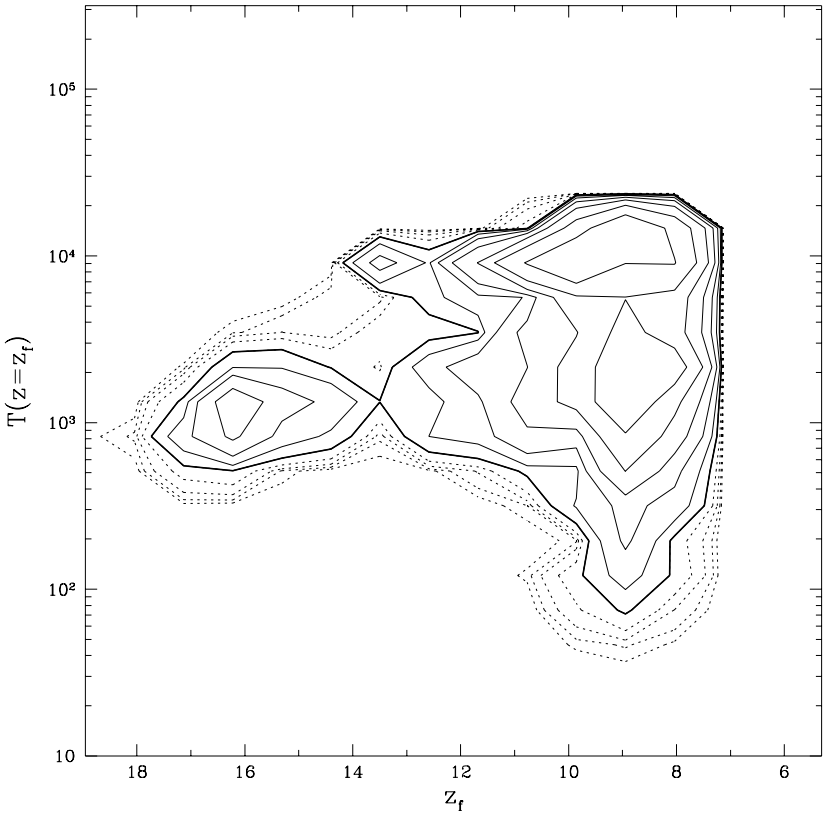

Fig. 5.— Joint distribution for all star particles in temperature and redshift at the moment and place of formation for run A. Two epochs of star formation: high z – low T and lower z – higher T are clearly distinguishable.

and photo-destruction, there was a relative pause in star formation until sometime around $z = 10$, when the fraction of objects with temperature in excess of 10^4 K became significant and hydrogen line cooling became the main cooling mechanism for Pop II star formation.

At each particular epoch the most massive objects are statistically the oldest, they formed first, accreted more mass and became Pop II objects before less massive ones. Therefore, at every particular moment it is the Pop II objects that are oldest, and the time-sequence of formation of Pop III and then Pop II objects is actually reversed, but it stems merely from the fact that the Pop III identification is temporary, and most Pop III objects will become Pop II objects with time. Since the run B barely shows the existence of Pop III objects, its mass resolution is apparently insufficient to resolve objects with the virial temperature of around 10^3 K, where the Pop III star formation occurs. We conclude therefore that mass resolution of the order of $10^4\,M_\odot$ is required in order to find Pop III objects in a simulation, and that in the real world it is likely that this population did form at redshift $z > 14$ leading to an early contamination of the universe with metals $\bar{Z}/Z_\odot \sim 10^{-3.7}$.

The authors would like to express their gratitude to Prof. Martin Rees for numerous fruitful

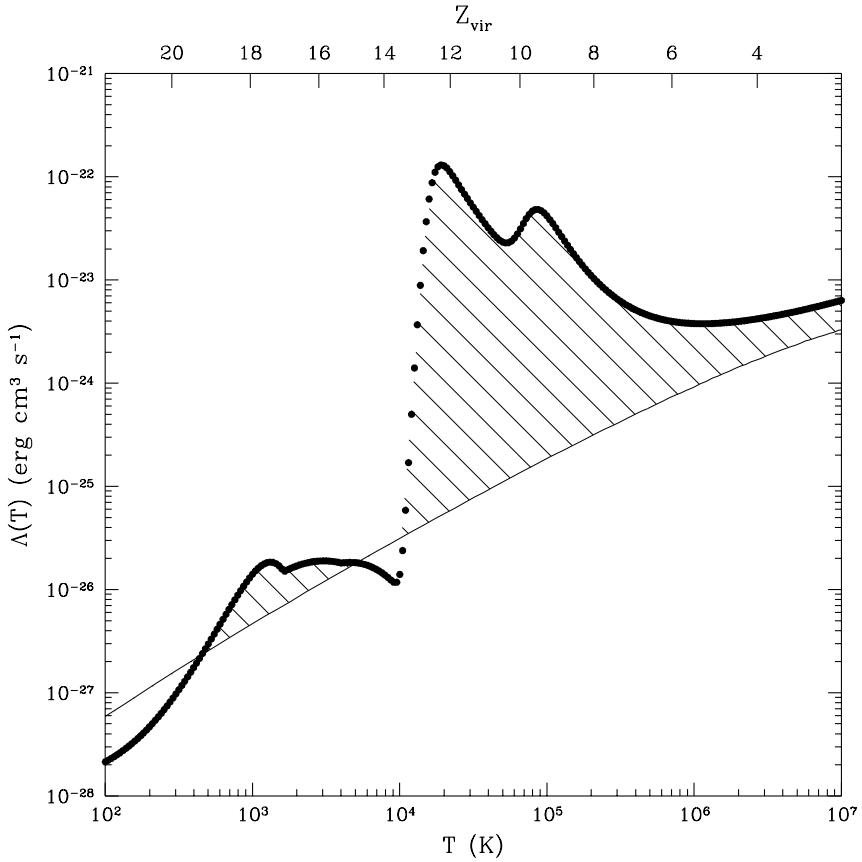

Fig. 6.— The cooling function for the primeval gas with the 10^{-3} molecular hydrogen abundance by mass (*heavy dots*). Shown with the thin line is the value of the cooling function required for a virialized 3σ peak with a given temperature to cool in a Hubble time. Note distinct epochs where H_2 band cooling or (H I,He II) line cooling permits collapse.

discussions and valuable comments. This work was supported by NSF grant AST-9318185 awarded to the Grand Challenge Cosmology Consortium.

REFERENCES

Bertschinger, E., and Gelb, J. 1991, Comp. in Phys., 5, 164

Cen, R., Ostriker, J. P., & Peebles, P. J. E. 1993, ApJ, 415, 423

Couchman, H. M. P., & Rees, M. J. 1986, MNRAS, 221, 53

Giallongo, E., D'Odorico, S., Fontana, A., McMahon, H. G., Savaglio, S., Cristiani, S., Molaro, P., & Treverse, D. 1994, ApJ, 425, L1

Giroux, M. L., & Shapiro, P. R. 1996, ApJS, 102, 191

Gnedin, N. Y. 1995, ApJS, 97, 231 (SLH)

Gnedin, N. Y., & Bertschinger, E. 1996, ApJ, submitted (astro-ph 9602063)

Gnedin, N. Y., & Ostriker, J. P. 1996, in preparation

Gunn, J. E., & Peterson, B. A. 1965, ApJ, 142, 1633

Jenkins, E. B., & Ostriker, J. P. 1991, ApJ, 376, 33

Kawasaki, M, & Fukugita, M. 1994, MNRAS, 269, 563

Ostriker, J. P., & Steinhardt, P. J. 1995, Nature, 377, 600

Peebles, P. J. E. 1993,*Principles of Physical Cosmology*, Princeton: Princeton University Press

Press, W. H. & Schechter, P. 1974, ApJ, 187, 425

Tegmark, M., & Silk, J. 1995, ApJ, 441, 458

——— 1994, ApJ, 423, 529

Tegmark, M., Silk, J., Rees, M. J., Blanchard, A., Abel, T., & Palla. F. 1996, ApJ, in press (astro-ph 9603007)